Analysis of the relationship between fringe angle and three-dimensional profilometry system sensitivity

Ping Zhou,* Xinran Liu, and Tongjing Zhu

School of Biological Science & Medical Engineering, Southeast University, Nanjing 210096, China

*Corresponding author: capzhou@163.com

The relationship between projector–camera baseline and the phase variation direction of fringe patterns is one of the essential characteristics in a three-dimensional (3D) profilometry system, although it has been ignored. This paper indicates that a 3D profilometry system will be most sensitive to object depth change when the phase variation direction of the fringe patterns is parallel to the baseline, which is analyzed in systems based on both the triangulation and stereovision principles. An efficient method is proposed to achieve the most sensitivity by projecting a set of fringe patterns of different phase variation directions. Experimental results demonstrate our analysis and the proposed determination method.   © 2014 Optical Society of America

OCIS codes: (120.0120) Instrumentation, measurement, and metrology; (120.2650) Fringe analysis; (100.5070) Phase retrieval.

http://dx.doi.org/10.1364/AO.53.002929

1. Introduction

Three-dimensional (3D) profilometry based on structured light is widely used in various domains, such as archaeological science, medical system, virtual reality, and reverse engineering [1–4]. The phase map corresponding to the depth variation of the object being measured has been one of the most important tools for reconstructing the 3D profiles of objects since it was introduced in 1983 [4–6]. During the past several decades, phase-based techniques have seen much development due to the contribution of a number of researchers in fringe pattern encoding methods, modified fringe analysis methods, phase unwrapping algorithms, calibration approaches, and so on [7–9].

Presently, there are two common approaches to calibrating the 3D profilometry system. The first one is based on the triangulation principle [5] and requires the projector–camera baseline to be parallel to the reference plane. An equation that relates the object depth to phase distribution is calibrated on the basis of system geometry. The second approach regards the projector as a reversed camera and uses the stereovision principle [10,11] to calibrate the geometric parameters of the experimental setups, even when the projector, camera, and objects are placed arbitrarily [11,12], which relaxes the constraint of the conventional optical geometry in the triangulation principle. Therefore, the 3D profilometry system based on the stereovision principle is most widely used. These two kinds of calibration methods can also be called the reference-plane method and the no-reference-plane method based on whether a reference plane is used or not [13]. Generally, both approaches simply project horizontal or vertical fringe patterns onto the object being measured to obtain the phase map. However, as improvement of the stereovision principle reduces the importance of the spatial relationship between the projector–camera baseline and the direction of fringe patterns, the

phase sensitivity to object depth variation is unfortunately ignored by most researchers. Wang and Zhang made some research and indicated that simply projecting horizontal or vertical fringe patterns is not the best option to obtain optimal sensitivity to object depth variations. They proposed a method to determine the optimal fringe angle by projecting a set of horizontal and vertical fringe patterns onto a step-height object [14]. To our knowledge, the mathematical analysis of the optimal fringe angle is still lacking in the systems based on either the triangulation principle or the stereovision principle.

In this paper, the optimal fringe angle is analyzed in both the triangulation and stereovision principles, and the specific expressions of the optimal fringe angle are obtained. Furthermore we propose and demonstrate that the optimal fringe angle is equal to the systematic angle that formed by the projector–camera baseline and horizontal direction when the 3D profilometry system is most sensitive. Subsequently, an efficient method to determine the systematic angle is proposed by projecting a set of fringe patterns with different directions. Finally, Experimental results are shown to demonstrate our theory and the validity of the method.

2. Fringe Angle Analysis

A. Triangulation Principle

An optical geometry of the 3D profilometry system based on triangulation is illustrated in Fig. 1 and mainly comprises a DLP digital projector and a CCD camera.

In the optical geometry, P and C denote the centers of the camera entrance pupil and the projector exit pupil, respectively. There is a rigorous restriction of the centers that P and C must be located at the same distance L from the reference plane ζ. That means the reference plane is parallel to the line PC, which is defined as the projector–camera baseline of the 3D profilometry system. Generally, the x axis is chosen to be parallel to the horizontal
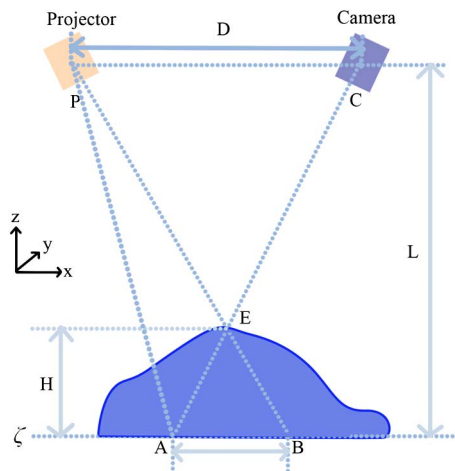

Fig. 1. 3D profilometry system model based on the triangulation principle.

direction, and the y axis is vertical to the plane of the figure. Obviously, the baseline is parallel to the x axis and the systematic angle formed by the baseline and the horizontal direction is zero.

If there is no measuring object, a principal ray of fringe patterns strikes the reference plane at point B, while for a general object with depth $H(x,y)$, the principal ray strikes the object surface at point E, and point E is observed to be point A on the reference plane by the camera, so that the fringe patterns are modulated by the object, which are captured by the camera and expressed as

$$g_0(x,y) = B(x,y) + A(x,y)\cos[\omega_0 x + \Delta\varphi(x,y)], \quad (1)$$

where $B(x,y)$ is average intensity, $A(x,y)$ is the intensity modulation, ω_0 is the fundamental frequency of the fringe patterns, and $\Delta\varphi$ is the phase change due to the object.

According to Takeda and Mutoh's theory [5], the phase change is expressed as

$$\Delta\varphi(x,y) = \varphi_A - \varphi_B = \omega_0\overline{AB}. \quad (2)$$

Noting that $\Delta EAB \backsim \Delta ECP$ in Fig. 1, there is

$$\frac{H(x,y)}{\overline{AB}} = \frac{L - H(x,y)}{D}, \quad (3)$$

where D is the distance between the centers of the projector and camera. Substituting Eq. (2) into Eq. (3) and solving it for $H(x,y)$, we can obtain

$$H(x,y) = \frac{\Delta\phi(x,y) \cdot L}{\Delta\phi(x,y) + \omega_0 D}. \quad (4)$$

Equation (4) can be expressed in another form:

$$\Delta\phi(x,y) = \omega_0 \frac{D \cdot H(x,y)}{L - H(x,y)}. \quad (5)$$

Equation (5) gives the relationship between the phase change and the distributions of depth. It also imposes an important restriction on the system that the baseline PC is parallel to the x axis in Fig. 1. Generally, fringe patterns are either horizontal or vertical in the imaging plane of camera. In our system, they are vertical, as shown in Fig. 2 (left stripes). Therefore, the phase variation direction of fringe patterns is parallel to the x axis and the baseline. It should be noted that the phase variation direction of fringe patterns is perpendicular to the direction of fringe patterns.

If fringe patterns are not vertical, in other words, there is an angle θ between the phase variation direction of the fringe patterns and the x axis, as shown in Fig. 2 (right stripes), which is denoted as the fringe angle. In that case, the frequency of fringe patterns is considered a vector: $\vec{\omega}_0 = \omega_x\vec{i} + \omega_y\vec{j}$.

Here, $\vec{i}$ and $\vec{j}$ are the unit vectors along the x and y axes, respectively. The orientation of ω_0 is the same
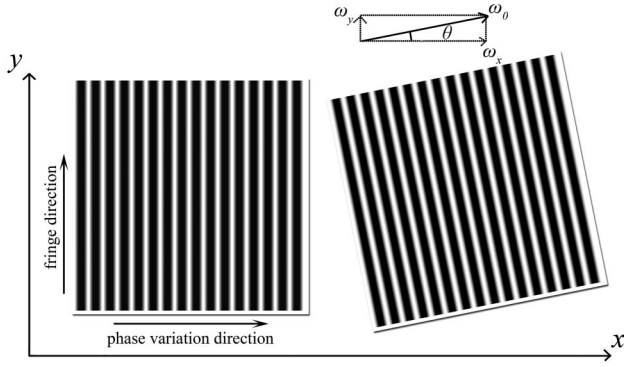
Fig. 2. Vertical fringe pattern (left) and oblique fringe pattern (right).

as the phase variation direction of the fringe patterns. When the fringe patterns are vertical, $\omega_0 = \omega_x$, $\omega_y = 0$, so Eq. (1) can be expressed as

$$g_0(x,y) = B(x,y) + A(x,y)\cos[\omega_x x + \Delta\varphi(x,y)]. \quad (6)$$

When the fringe angle θ exists and ω_y is not zero, the modulated fringe patterns captured by the camera are expressed as

$$g_0'(x,y) = B(x,y) + A(x,y)\cos[\omega_x x + \omega_y y + \Delta\varphi'(x,y)], \quad (7)$$

where $\omega_x = \omega_0 \cdot \cos\theta$, $\omega_y = \omega_0 \cdot \sin\theta$, and $\Delta\varphi'(x,y)$ is still the phase change due to the object. However, the phase change has nothing to do with the component in the y axis, as shown in Fig. 1, so that the phase change is described as

$$\Delta\varphi'(x,y) = \Delta\varphi'(x) = \omega_x \frac{D \cdot H(x,y)}{L - H(x,y)}$$
$$= \omega_0 \cos\theta \cdot \frac{D \cdot H(x,y)}{L - H(x,y)}. \quad (8)$$

To provide the best sensitivity to object depth variation, the maximum $\partial\Delta\varphi/\partial H$ is needed. For a given depth H, as the coefficients D, L, and ω_0 are all constant, the 3D profilometry system obviously reaches its highest sensitivity when the fringe angle θ is zero. In that case, the fringe angle is equal to the systematic angle, i.e., the phase variation direction of fringe patterns is parallel to the baseline PC. Conversely, if the fringe angle is $\pi/2$ or the phase variation direction of the fringe patterns is perpendicular to the baseline PC, the phase change is always zero, whatever the object depth variation is. In that case, the 3D profilometry system is the least sensitive to the object depth. In practice, it is difficult to confirm the direction of the projector–camera baseline so that the systematic angle is not usually zero. Although it is easy to obtain a fringe angle of zero by projecting vertical fringe patterns, it is not equal to the systematic angle. Hence, the fringe patterns need to be projected at an optimal angle to ensure that the fringe

angle is equal to the systematic angle, just as Wang and Zhang did [14].

B. Stereovision Principle

The common pinhole camera model is adopted for both camera and projector in the stereovision principle, as the projector can be conceptually regarded as a reversed camera. As shown in Fig. 3, O_w-$X_w Y_w Z_w$ is the world coordinate system, O_c-$X_c Y_c Z_c$ is the camera coordinate system, and O_p-$X_p Y_p Z_p$ is the projector coordinate system. Q is a point with world coordinate $Q_w = [x_w, y_w, z_w]^T$ in 3D space; it can be transformed into the camera and projector coordinate system by applying Eq. (9):

$$\begin{cases} Q_c = R \cdot Q_w + T \\ Q_p = M \cdot Q_w + P \end{cases}, \quad (9)$$

where

$$R = \begin{bmatrix} r_1 & r_2 & r_3 \\ r_4 & r_5 & r_6 \\ r_7 & r_8 & r_9 \end{bmatrix}, \qquad M = \begin{bmatrix} m_1 & m_2 & m_3 \\ m_4 & m_5 & m_6 \\ m_7 & m_8 & m_9 \end{bmatrix}$$

are 3-by-3 rotation matrices for the camera and projector, respectively. $T = [t_1, t_2, t_3]^T$ and $P = [p_1, p_2, p_3]^T$ are corresponding shift vectors.

Then, a projective transformation of the point Q with coordinates $Q_c = [x_c, y_c, z_c]^T$ to the camera normalized image coordinates $[X, Y]^T$ is processed. Moreover, the point Q is located in an equiphase plane of the projector with projector normalized image coordinate Φ. Three equations can be established:
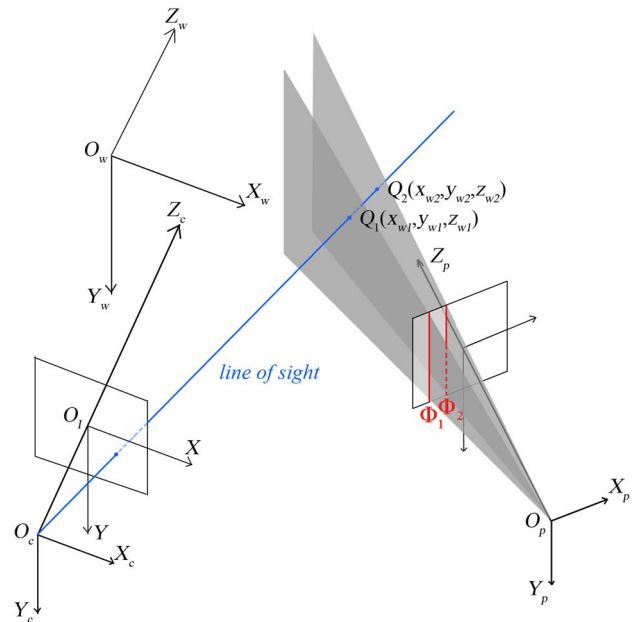

Fig. 3. 3D profilometry system model based on the stereovision principle.

$$\begin{cases} X = f_{cx} \cdot x_c/z_c \\ Y = f_{cy} \cdot y_c/z_c \\ \Phi = f_{px} \cdot x_p/z_p \end{cases} \quad (10)$$

where f_{cx} and f_{cy} are the focal lengths of the camera on the x axis and y axis, respectively, and f_{px} is the focal length of the projector on the x axis. For each equiphase plane of the projector, the normalized image coordinate Φ can be transformed into absolute phase value φ of the fringe [15]. This linear relationship can be denoted as $\Phi = f(\varphi)$. By substituting Eq. (9) into Eq. (10), we can obtain

$$X = f_{cx} \frac{r_1 x_w + r_2 y_w + r_3 z_w + t_1}{r_7 x_w + r_8 y_w + r_9 z_w + t_3}, \quad (11)$$

$$Y = f_{cy} \frac{r_4 x_w + r_5 y_w + r_6 z_w + t_2}{r_7 x_w + r_8 y_w + r_9 z_w + t_3}, \quad (12)$$

$$\Phi = f_{px} \frac{m_1 x_w + m_2 y_w + m_3 z_w + p_1}{m_7 x_w + m_8 y_w + m_9 z_w + p_3}. \quad (13)$$

For each specific "line of sight," the normalized image coordinates $[X, Y]^T$ are constant. By setting $k_1 = X/f_{cx}, k_2 = Y/f_{cy}, x_w,$ and y_w can be expressed as

$$x_w = a_1 z_w + a_0, \quad (14)$$

$$y_w = b_1 z_w + b_0, \quad (15)$$

where $a_1, a_0, b_1,$ and b_0 are constant:

$$a_1 = \frac{(k_2 r_9 - r_6)(k_1 r_8 - r_2) - (k_1 r_9 - r_3)(k_2 r_8 - r_5)}{(k_1 r_7 - r_1)(k_2 r_8 - r_5) - (k_2 r_7 - r_4)(k_1 r_8 - r_2)}, \quad (16)$$

$$a_0 = \frac{(k_2 t_3 - t_2)(k_1 r_8 - r_2) - (k_1 t_3 - t_1)(k_2 r_8 - r_5)}{(k_1 r_7 - r_1)(k_2 r_8 - r_5) - (k_2 r_7 - r_4)(k_1 r_8 - r_2)}, \quad (17)$$

$$b_1 = \frac{(k_2 r_9 - r_6)(k_1 r_7 - r_1) - (k_1 r_9 - r_3)(k_2 r_7 - r_4)}{(k_1 r_8 - r_2)(k_2 r_7 - r_4) - (k_2 r_8 - r_5)(k_1 r_7 - r_1)}, \quad (18)$$

$$b_0 = \frac{(k_2 t_3 - t_2)(k_1 r_7 - r_1) - (k_1 t_3 - t_1)(k_2 r_7 - r_4)}{(k_1 r_8 - r_2)(k_2 r_7 - r_4) - (k_2 r_8 - r_5)(k_1 r_7 - r_1)}. \quad (19)$$

When the line of sight sequentially pierces the equiphase planes of the projector, monotonically changing phase values are obtained. By substituting Eqs. (14) and (15) into Eq. (13), we can obtain a phase-to-depth relationship in the stereovision principle:

$$\Phi = f_{px} \frac{(a_1 m_1 + b_1 m_2 + m_3)z_w + (a_0 m_1 + b_0 m_2 + p_1)}{(a_1 m_7 + b_1 m_8 + m_9)z_w + (a_0 m_7 + b_0 m_8 + p_3)}. \quad (20)$$

To simplify Eq. (20), we can write

$$\Phi = f_{px} \frac{n_1 z_w + n_0}{s_1 z_w + s_0}. \quad (21)$$

As shown in Fig. 3, two points Q_1, Q_2 lying on the line of sight are at different depths and different equiphase planes. The normalized image coordinate change is

$$\begin{aligned} \Delta\Phi &= \Phi_1 - \Phi_2 \\ &= f_{px} \frac{n_0 s_1 - n_1 s_0}{s_1^2} \cdot \frac{z_{w2} - z_{w1}}{\left(z_{w1} + \frac{s_0}{s_1}\right)\left(z_{w2} + \frac{s_0}{s_1}\right)}. \end{aligned} \quad (22)$$

If the position of Q_1, Q_2 is fixed, the larger $\Delta\Phi$ we have, the larger phase change we get, and the more sensitive to depth variation our system will be. According to Eq. (22), this sensitivity is related to the projector extrinsic parameter M, P as $a_1, a_0, b_1,$ and b_0 are constant. That means if the projector and camera are placed arbitrarily, it may not be the most sensitive condition for the system.

C. Error Analysis

Ideally, the system is linear. However, error and distortion always exist in practice. There are two main error sources that cannot be neglected: system nonlinear response (i.e., gamma distortion) and projection-imaging distortion of the lens [16].

The system nonlinear response distorts the phase value with a sinusoidal phase error distribution [8,17]. Usually, this distortion can be eliminated effectively by a gamma pre-encoding process [18]. The projection-imaging distortion of a lens makes the relationship between absolute phase value φ and normalized image coordinate Φ nonlinear. This distortion can be modeled as several system internal parameters in the system calibration process and subsequently corrected.

Nevertheless, the error cannot be eliminated completely. There will be tiny residual phase error during the measurement. According to Eqs. (8) and (22), if the sensitivity of phase change to depth variation is small, even a tiny phase error will lead to large depth fluctuation, which will reduce measurement accuracy. Therefore, to restrain the error and achieve high reconstruction precision, the sensitivity of the system should be as high as possible.

3. Simulation of Fringe Angle in the Stereovision Principle

In Wang and Zhang's work [14], they demonstrated the existence of the optimal fringe angle by experiment with the help of a reference plane and proposed a simple method to determine the optimal fringe angle. The corresponding mathematical analysis is

given in Section [2.A](#). Thus, we mainly focus on the optimal fringe angle in the stereovision principle in this paper. A simulation is performed to illustrate the relationship between fringe angle and the sensitivity of phase change to depth variation.

We use a camera and a digital projector to constitute a 3D profilometry system. The devices are placed arbitrarily and then calibrated on the basis of the stereovision principle [15]. The calibration result is shown in Fig. [4](#). It is clear that the camera and projector are not at the same horizontal position. The systematic angle formed by the projector–camera baseline and the x axis is 25.51°.

To reveal the relationship between fringe angle and system sensitivity quantitatively, we rotate the projector around its optical axis at different fringe angles. If the projector is rotated θ, the rotation matrix and shift vector become

$$[M' \quad P'] = \begin{bmatrix} \cos\theta & -\sin\theta & 0 \\ \sin\theta & \cos\theta & 0 \\ 0 & 0 & 1 \end{bmatrix} [M \quad P], \qquad (23)$$

where

$$M' = \begin{bmatrix} m_1\cos\theta - m_4\sin\theta & m_2\cos\theta - m_5\sin\theta & m_3\cos\theta - m_6\sin\theta \\ m_1\sin\theta + m_4\cos\theta & m_2\sin\theta + m_5\cos\theta & m_3\sin\theta - m_6\cos\theta \\ m_7 & m_8 & m_9 \end{bmatrix}. \qquad (24)$$

$$P' = \begin{bmatrix} p_1\cos\theta - p_2\sin\theta \\ p_1\sin\theta + p_2\cos\theta \\ p_3 \end{bmatrix} \qquad (25)$$

To simulate a given depth variation, we set $z_{w1} = 0$ mm, $z_{w2} = 200$ mm and substitute Eqs. ([24](#)) and ([25](#)) into Eq. ([22](#)). The normalized image coordinate change $\Delta\Phi$ is shown in Fig. [5](#), with different rotation angle θ from 0° to 180°.

The result shows that the 3D profilometry system is not the most sensitive to this given depth variation when the fringe angle is zero. $\Delta\Phi$ reaches its peak when the fringe angle is 24.8°, which is very close to the systematic angle of our system. In that
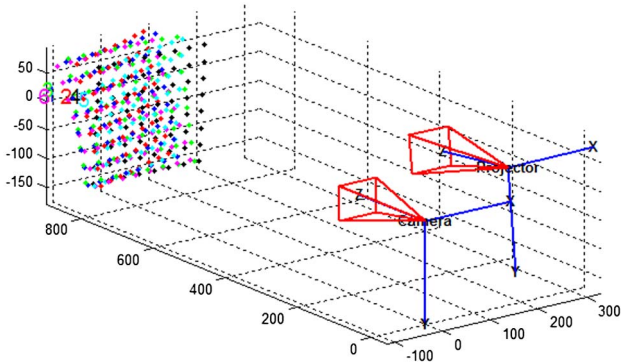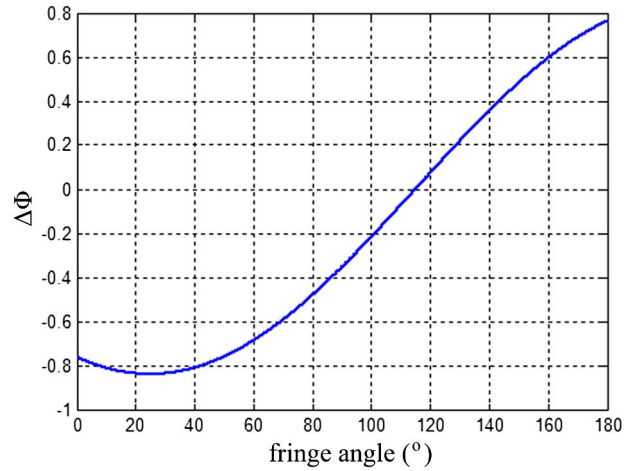

Fig. 5.   Simulation result of the relationship between normalized image coordinate change and fringe angle.

case, the 3D profilometry system reaches its best performance. When the fringe angle is equal to the systematic angle, the phase variation direction of the projected fringe patterns will be parallel to the baseline of the camera and projector. On the other hand, $\Delta\Phi$ is close to zero when the fringe angle θ is 114.8°, which means the system is least sensitive to depth variation. Thus, whatever the measured object depth is, the absolute phase value will not change and it is impossible to reconstruct the surface of the object.

4. Experimental Results and Discussion

Our employed 3D profilometry system is composed of a BenQ GP1 projector and Microvision VD120SC
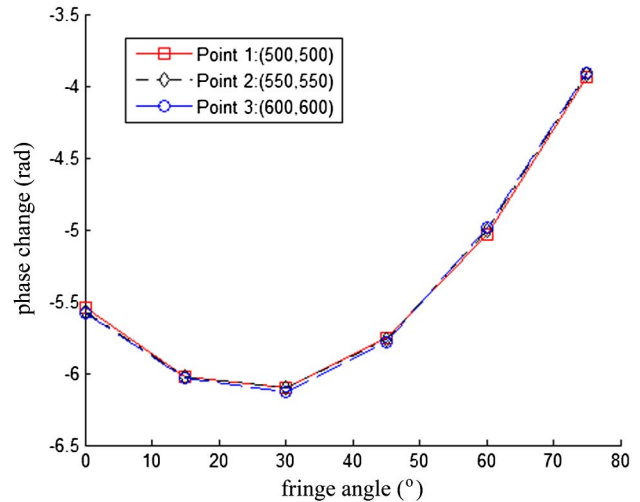

Fig. 6.   Experimental results of the relationship between phase change and fringe angle.

Fig. 4.   Calibration result of the 3D profilometry system.

camera. The positions of projector and camera are as shown in Fig. 4. Several experiments are performed to verify the phenomenon we analyze in this paper and the existence of optimal fringe angle in the stereovision principle.

To eliminate the gamma effect of the projector, both a gamma pre-encoding process and a 16-step phase-shifting method [17] are used in our experiments. First, a flat board is measured by projecting fringe patterns at different fringe angles: 0°, 15°, 30°,
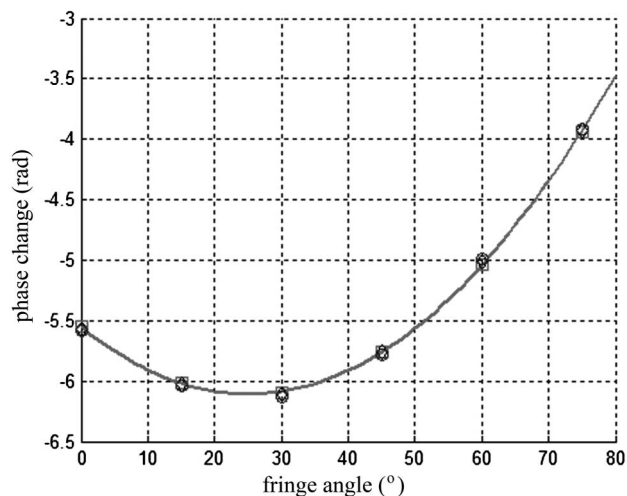

Fig. 7. Curve fitting result.

45°, 60°, and 75°, and the absolute phase map is achieved. Second, this flat board is moved forward about 200 mm and the measuring procedures mentioned above are implemented again. In both absolute phase maps, we select three points (500, 500), (550, 550), and (600, 600), that is, three lines of sight as shown in Fig. 3. The relationship between the phase changes due to these two depths and fringe angles is shown in Fig. 6.

As the positions of the flat board before and after movement are approximately parallel, there are similar depth variations in these three points and the phase changes under the same fringe angle are almost equal. Moreover, an important result is achieved that, when the fringe patterns with different fringe angles are projected, the phase changes are obviously different, which perfectly demonstrates our analysis in this paper. As shown in Fig. 6, the phase change is largest when the fringe angle is 30°. To determine the optimal fringe angle accurately, the polynomial fitting method is performed.

As depicted in Fig. 7, the curve reaches its peak when the fringe angle is 26.0°. Therefore, the optimal fringe angle of the 3D profilometry system is 26.0°, which is close to the systematic angle 25.5° and agrees well with the simulation result of 24.8° that we obtained in Section 3. The result also reveals that, although the stereovision-principle-based calibration method allows placing the devices and object arbitrarily, the 3D profilometry system may not be
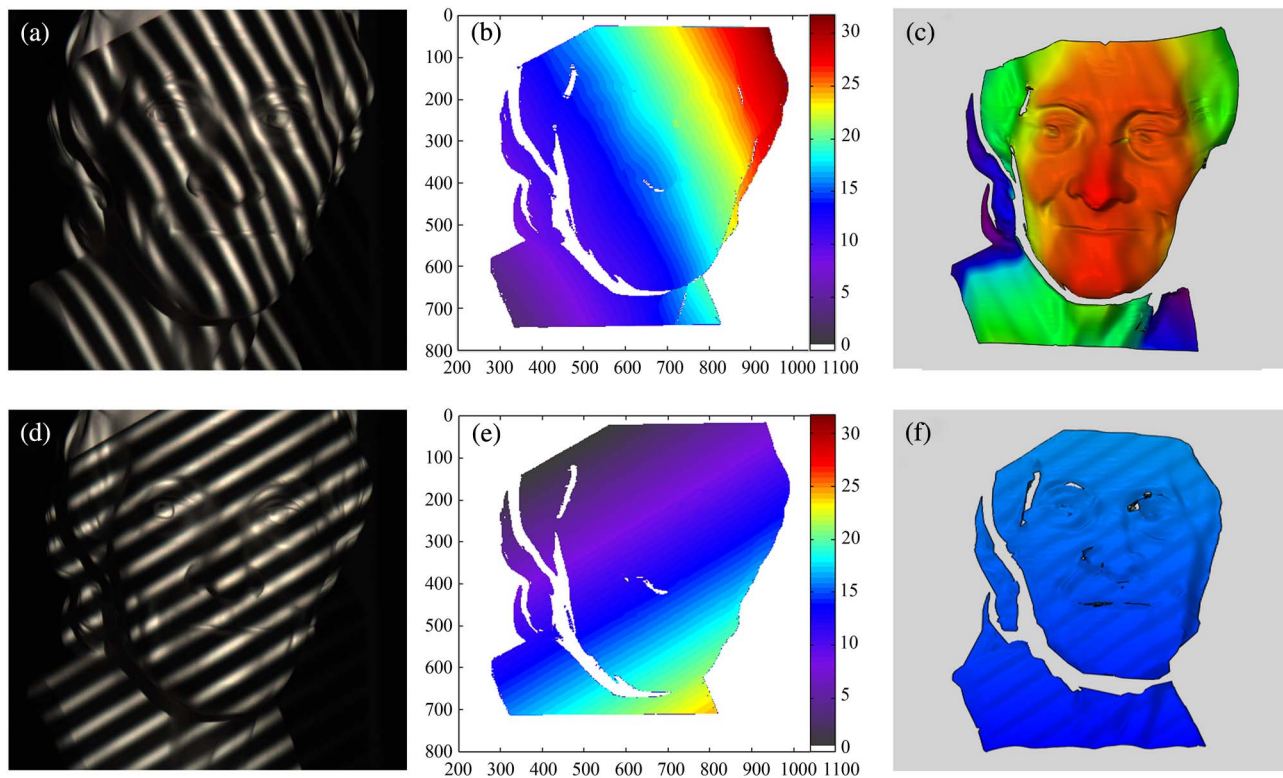

Fig. 8. Experimental results of sculpture. (a) The captured image when the system has optimal sensitivity. (b) The retrieved phase map of (a). (c) Reconstructed 3D shape of (a). (d) The captured image when the system has the worst sensitivity. (e) The retrieved phase map of (d). (f) Reconstructed 3D shape of (d).

the most sensitive to object depth variation. To achieve the most sensitivity, the optimal fringe angle should be equal to the systematic angle, i.e., the phase variation direction of the fringe patterns should be parallel to the projector–camera baseline. Furthermore, if horizontal or vertical fringe patterns are projected, it is better to ensure that the projector–camera baseline is vertical or horizontal, also.

Subsequently, a more complex object is measured while the system has optimal sensitivity and the worst sensitivity. The captured images and retrieved results under these two conditions are shown in Fig. 8. Figures 8(a) and 8(b) show that the fringe strips are obviously distorted by the depth variation. Also, highly detailed phase-to-depth mapping information is depicted in the phase map. In contrast, the fringe strips in Fig. 8(d) are approximately paralleled, and the phase map in Fig. 8(e) cannot reflect the depth information at all. Figures 8(c) and 8(f) show the best and worst reconstructed 3D shapes, respectively. When the system has optimal sensitivity, the sculpture can be reconstructed in detail with little error. However, when the system has the worst sensitivity, there are obviously sinusoidal ripples on the result, even though efficient methods are used to restrain the phase error, and the height information of the sculpture is totally wrong.

5. Conclusion

In this paper, it is indicated that simply projecting horizontal or vertical fringe patterns is not highly sensitive to object height for a given structured light system, as the projector–camera baseline is uncertain in practice and a systematic angle usually exists. To achieve the highest sensitivity of our 3D profilometry system, we analyzed the relationship between fringe angle and system sensitivity in both the triangulation and stereovision principles. It is demonstrated that the optimal fringe angle is equal to the systematic angle when the system is most sensitive to depth variance and least sensitive to error. In other words, the phase variation direction of fringe patterns should be parallel to the projector–camera baseline. We have proposed a method to determine the optimal fringe angle accurately and demonstrated the efficiency of the method by experimental results.

References

1. S. C. Park and M. Chang, "Reverse engineering with a structured light system," Comput. Ind. Eng. **57**, 1377–1384 (2009).
2. L. Niven, T. E. Steele, H. Finke, T. Gernat, and J. Hublin, "Virtual skeletons: using a structured light scanner to create a 3D faunal comparative collection," J. Archaeol. Sci. **36**, 2018–2023 (2009).
3. H. Guo and P. Huang, "Face recognition based on fringe pattern analysis," Opt. Eng. **49**, 037201 (2010).
4. S. Zhang, "Recent progresses on real-time 3D shape measurement using digital fringe projection techniques," Opt. Lasers Eng. **48**, 149–158 (2010).
5. M. Takeda and K. Mutoh, "Fourier transform profilometry for the automatic measurement of 3D object shapes," Appl. Opt. **22**, 3977–3982 (1983).
6. Y. Wang, K. Liu, Q. Hao, D. L. Lau, and L. G. Hassebrook, "Period coded phase shifting strategy for real-time 3D structured light illumination," IEEE Trans. Image Process. **20**, 3001–3013 (2011).
7. K. Xue, Y. Li, S. Lu, and L. Chen, "Three-dimensional shape measurement using improved binary spatio-temporal encoded illumination and voting algorithm," Appl. Opt. **50**, 5508–5512 (2011).
8. B. Pan, Q. Kemao, L. Huang, and A. Asundi, "Phase error analysis and compensation for nonsinusoidal waveforms in phase-shifting digital fringe projection profilometry," Opt. Lett. **34**, 416–418 (2009).
9. S. Fang, L. Meng, L. Wang, P. Yang, and M. Komori, "Quality-guided phase unwrapping algorithm based on reliability evaluation," Appl. Opt. **50**, 5446–5452 (2011).
10. R. Yang, S. Cheng, and Y. Chen, "Flexible and accurate implementation of a binocular structured light system," Opt. Lasers Eng. **46**, 373–379 (2008).
11. M. Vo, Z. Wang, T. Hoang, and D. Nguyen, "Flexible calibration technique for fringe-projection-based three-dimensional imaging," Opt. Lett. **35**, 3192–3194 (2010).
12. H. Cui, W. Liao, N. Dai, and X. Cheng, "A flexible and rapid micro-adjustment algorithm for structured light 3D measurement system with camera-projector," Optik **123**, 109–116 (2012).
13. S. Cui and X. Zhu, "A generalized reference-plane-based calibration method in optical triangular profilometry," Opt. Express **17**, 20735–20746 (2009).
14. Y. Wang and S. Zhang, "Optimal fringe angle selection for digital fringe projection technique," Appl. Opt. **52**, 7094–7098 (2013).
15. Z. Li, Y. Shi, C. Wang, and Y. Wang, "Accurate calibration method for a structured light system," Opt. Eng. **47**, 053604 (2008).
16. S. Ma, R. Zhu, C. Quan, L. Chen, C. J. Tay, and B. Li, "Flexible structured-light-based three-dimensional profile reconstruction method considering lens projection-imaging distortion," Appl. Opt. **51**, 2419–2428 (2012).
17. K. Liu, Y. Wang, D. L. Lau, Q. Hao, and L. G. Hassebrook, "Gamma model and its analysis for phase measuring profilometry," J. Opt. Soc. Am. A **27**, 553–562 (2010).
18. T. Hoang, B. Pan, D. Nguyen, and Z. Wang, "Generic gamma correction for accuracy enhancement in fringe-projection profilometry," Opt. Lett. **35**, 1992–1994 (2010).